Measurement and Characterization of Entropy and Degree of Polarization of Weather Radar Targets

Michele Galletti, David H. O. Bebbington, Madhu Chandra, and Thomas Börner

***Abstract*—To date, few polarimetric weather radars have exhibited the capability to measure full scattering matrices. In contrast, in the synthetic aperture radar (SAR) community, considerable experience has been gained in dealing with complete scattering matrices and their statistical behavior. This paper aims to place weather radar parameters in a wider context in order to exploit more general concepts like target decomposition theorems and polarization basis transformations. Entropy, which is a fully polarimetric variable derived from the Cloude–Pottier decomposition, and the degree of polarization, which is derived from Wolf's coherence matrix, are the subject of this paper. The theoretical analysis carried out in the first part is checked against fully polarimetric data from POLDIRAD, which is the German Aerospace Center research weather radar. The entropy and the degree of polarization are compared with the copolar correlation coefficient in order to understand whether they can add value to radar meteorological investigations. Because the degree of polarization is available to conventional dual-polarization coherent systems, it is important to assess its potential for operational use.**

***Index Terms*—Degree of polarization, depolarization response, instantaneous scattering matrix (ISM), scattering matrix, target decomposition (TD) theorems.**

I. Introduction

A FULLY polarimetric radar is able to transmit pulses whose polarization state is switched every pulse repetition interval [henceforth pulse repetition time (PRT)] and set to simultaneously receive the copolar and cross-polar components of the backscattered signal (dual receiver). Such setup allows quasi-simultaneous measurements of the scattering matrix. The first meteorological radar designed to measure complete scattering matrices of weather targets was developed at the German Aerospace Center (DLR) about 20 years ago and known to the weather radar community as POLDIRAD. The term polarization diversity refers to its capability of being able to fast switch on transmit between any pair of orthogonal polarization states. For a detailed technical description of the system, we refer to [1]. To collect the data presented in this paper, POLDIRAD was operated to switch between horizontal and vertical polarization states on transmit and set to receive the copolar and cross-polar components of the backscattered signal. Ideally, all elements of a scattering matrix should be measured simultaneously. However, because (unless some coding schemes can be used) the transmit polarizations must be emitted sequentially, the scattering matrix measured by a fully polarimetric weather radar is affected by both the mean motion of the target and the decorrelation due to random displacements of the single scatterers. Mean motion results in a phase offset between the first and second columns of the scattering matrix, whereas random motion manifests itself in amplitude and phase fluctuations of the backscattered signal. If the second effect cannot be corrected, special signal processing procedures must be applied to correct for the Doppler phase shift [2], [3].

From a set of scattering matrices, the covariance matrix can be built [4]–[6], and from the latter, it is possible to derive radar meteorological variables like reflectivity (Z_{HH}), differential reflectivity (Z_{DR}), linear depolarization ratio (LDR), differential phase (Φ_{DP}), or the copolar correlation coefficient ($|\rho_{h\nu}(0)|$). We refer to [5] and [6] for a detailed description of variables that are in use in radar meteorology. Furthermore, considering that the upper left and lower right 2×2 minors of the covariance matrix constitute the two Wolf's coherence matrices for the transmit states in use by the system, the corresponding degrees of polarization can be extracted.

If the full covariance matrix is available, more sophisticated signal processing procedures can be envisioned like polarization basis transformations or the application of target decomposition (TD) theorems [7]–[18].

The TD theorems can be divided into coherent and incoherent theorems. Among the first group rank Cameron, Pauli, and Krogager, whereas among the second, we find the Huynen–Barnes and the Cloude–Pottier decompositions. Every TD theorem is rather application dependent, and its use is subject to a careful analysis of the observed scene. Given the highly incoherent nature of hydrometeors, our investigation is directed toward variables developed for the study of incoherent targets. In the frame of radar meteorology, the term incoherent refers to the short decorrelation time of weather targets. At microwave wavelengths, such time is on the order of milliseconds with a dependence on wavelength, hydrometeor type, and turbulence in the resolution volume.

In this paper, we derive analytical results and examine experimental data to comparatively investigate the properties of entropy (H), degree of polarization (p), and the copolar correlation coefficient ($|\rho_{h\nu}(0)|$). The latter variable is well known to the weather radar community and defined as

$$\rho_{h\nu}(0) = \frac{\langle S_{hh} S_{\nu\nu}^{*} \rangle}{\sqrt{\langle |S_{hh}|^2 \rangle \langle |S_{\nu\nu}|^2 \rangle}}. \tag{1}$$

Manuscript received August 31, 2007; revised January 9, 2008. Current version published October 1, 2008. This work was supported by the European Union Project AMPER, Application of Multiparameter Polarimetry in Environmental Remote Sensing.

M. Galletti and T. Börner are with the Microwaves and Radar Institute, German Aerospace Center, 82234 Wessling, Germany (e-mail: michele.galletti@dlr.de).

D. H. O. Bebbington is with the Department of Electronic Systems Engineering, University of Essex, CO4 3SQ Colchester, U.K.

M. Chandra is with the Department of Microwave Engineering and Photonics, Chemnitz University of Technology, 09126 Chemnitz, Germany.

Color versions of one or more of the figures in this paper are available online at http://ieeexplore.ieee.org.

Digital Object Identifier 10.1109/TGRS.2008.920910

It is mainly sensitive to the variability in the ratio of the vertical-to-horizontal size of the illuminated particles. Entropy is sensitive to the heterogeneity of the scattering matrices that come in the formation of the covariance matrix, and it can be obtained only from a fully polarimetric system. The degree of polarization is sensitive to the variability of the Jones vectors that come in the formation of Wolf's coherence matrix and obtainable from a dual-polarization coherent system [19]. Contrary to the degree of polarization or the copolar correlation coefficient, entropy is sensitive to the whole polarimetric heterogeneity that is present in the resolution volume, and it can be used to measure how well the depolarizing properties of an incoherent target are captured by simpler dual-polarization variables. In this perspective, the concept of depolarization response is introduced in order to illustrate the degree of polarization dependence on transmit-polarization state. For this investigation, unitary transformations are used to obtain, from fully polarimetric data, the degrees of polarization corresponding to different transmit states.

The objectives of this paper can be itemized as follows.

1) Evaluate the performance of entropy and the degree of polarization for radar meteorological purposes, like hydrometeor identification or clutter detection. In particular, sensitivity to depolarizing effects from rain at C-band is investigated.
2) Assess the potential of the degree of polarization for operational use. Being measurable by dual-polarization coherent systems, it is important to assess whether it can complement the information that is obtainable from the set of variables that are normally available.

This paper is organized as follows. Section II reports the signal processing procedures applied to obtain instantaneous scattering matrices. Section III contains theoretical considerations about the degree of polarization, entropy, and the copolar correlation coefficient. In Section IV, experimental data are shown for one convective and one stratiform events, and the earlier itemized issues are addressed by confronting theory and data. The results are then summarized in Section V.

II. Construction of the ISM

The first step to obtain calibrated matrices involves the correction of hardware offset phases. The second step corrects the quasi-instantaneous scattering matrices for Doppler phase shift [2]. We start with the latter.

A. ISM Estimation

In the case of a fully polarimetric weather radar like POLDIRAD, the two columns of the scattering matrix S are measured at one pulse lag

$$S = \begin{bmatrix} S_{HH}(t+PRT) & S_{HV}(t) \\ S_{VH}(t+PRT) & S_{VV}(t) \end{bmatrix}. \tag{2}$$

At a given time instant, only two terms are actually measured, and two others are needed to be estimated. For simplicity, we consider the measurement done at time t and illustrate the procedures to interpolate the two missing terms. As far as the missing cross-polar term is concerned, reciprocity can be invoked, and no interpolation is needed. For the missing copolar term, the following procedures can be envisioned.

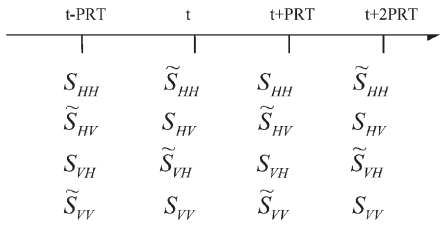

Fig. 1. Schematic representation of the alternating pulsing scheme for a fully polarimetric radar. Tildes indicate the estimated (missing) terms.

As proposed in [2], to estimate the amplitude, a simple interpolation can be used or a full sequence of temporal samples can be considered for a higher order polynomial fit

$$\left|\widetilde{S}_{HH}(t)\right| = \frac{1}{2}\left\{|S_{HH}(t-prt)| + |S_{HH}(t+prt)|\right\}. \tag{3}$$

As far as the phase is concerned, the same technique can be used [2]

$$\arg\{\tilde{S}_{HH}\} = \frac{1}{2}\left[\arg\{S_{HH}(t-prt)\} + \arg\{S_{HH}(t+prt)\}\right]. \tag{4}$$

As pointed out in [2], using only two samples might render the procedure vulnerable to system phase noise, and averaging can be considered for phase estimation.

The first approach involves the following quantities, which are separated by two pulse lags:

$$\hat{\Phi}^{HHHH}_{\mathrm{DOPPLER}} = \frac{1}{2}\arg\left[\sum_{n=1}^{N-1} S_{HH}[2n-1]\left(S_{HH}[2n+1]\right)^*\right] \tag{5}$$

$$\hat{\Phi}^{VVVV}_{\mathrm{DOPPLER}} = \frac{1}{2}\arg\left[\sum_{n=1}^{N-1} S_{VV}[2n]\left(S_{VV}[2n+2]\right)^*\right]. \tag{6}$$

Here, $\hat{\Phi}^{HHHH}_{\mathrm{DOPPLER}}$ and $\hat{\Phi}^{VVVV}_{\mathrm{DOPPLER}}$ are the estimated Doppler phase shifts at one pulse lag at horizontal and vertical polarizations, respectively.

With reference to Fig. 1, considering a scattering matrix measured by two successive pulses, the correction to obtain the instantaneous scattering matrix (ism) is performed as follows (reciprocity is invoked, and amplitude correction is not performed):

$$\begin{bmatrix} S_{HH}(t+prt) & S_{HV}(t) \\ S_{VH}(t+prt) & S_{VV}(t) \end{bmatrix} \rightarrow \begin{bmatrix} S_{HH}(t+prt)e^{+i\hat{\Phi}^{HHHH}_{\mathrm{DOPPLER}}} & S_{HV}(t) \\ S_{HV}(t) & S_{VV}(t) \end{bmatrix} \tag{7}$$

$$\begin{bmatrix} S_{HH}(t+prt) & S_{HV}(t) \\ S_{VH}(t+prt) & S_{VV}(t) \end{bmatrix} \rightarrow \begin{bmatrix} S_{HH}(t+prt) & S_{VH}(t+prt) \\ S_{VH}(t+prt) & S_{VV}(t)e^{-i\hat{\Phi}^{VVVV}_{\mathrm{DOPPLER}}} \end{bmatrix}. \tag{8}$$

We can either tune the first column to the same time instant as the second or, alternatively, tune the second column to the same time instant as the first [(7) and (8)]. Another possibility is to shift each by one-half pulse lag. The latter approach might have

an advantage point because, as the autocorrelation function is quadratic near the origin, the effects of decorrelation may be proportional to the square of the time interval.

If the two quantities appearing in (5) and (6) have approximately the same value, some observations can be made. The condition that satisfies this equality is that the phase center displacement over a pulse lag must be the same at horizontal and vertical polarizations. From a physical viewpoint, this is equivalent to the condition that the scatterers' anisotropy and line-of-sight velocity be decoupled. The formulas in (5) and (6) involve quantities separated by two pulse lags. If the difference between $\hat{\Phi}^{HHHH}_{\mathrm{DOPPLER}}$ and $\hat{\Phi}^{VVVV}_{\mathrm{DOPPLER}}$ is not too large, it is preferable to use estimators relying on quantities separated by just one pulse lag. Such estimator can be used instead of (5) or (6) and can be computed as follows [2]:

$$\Phi^{HHVV}_{\mathrm{DOPPLER}} = \frac{1}{2}(\widetilde{\Psi}_2 + \widetilde{\Psi}_1) \tag{9}$$

$$\widetilde{\Psi}_1 = \arg\left[\sum_{n=1}^{N-1} S_{HH}[2n+1]\,(S_{VV}[2n])^*\right] \tag{10}$$

$$\widetilde{\Psi}_2 = \arg\left[\sum_{n=1}^{N} S_{VV}[2n]\,(S_{HH}[2n-1])^*\right]. \tag{11}$$

The Doppler phase shift corrections illustrated in this paper must be implemented if the scattering matrices have to be used "as such," for example, when a unitary rotation is performed to transform scattering matrices to another polarization basis or TD theorems are applied. As far as entropy is concerned, a couple of remarks might be helpful. The amplitude correction reported earlier slightly influences its value. However, the tests performed with POLDIRAD data show that these variations hardly ever exceed 0.03–0.04 in worst cases. Phase corrections do not alter at all its value. This fact will be explained in Section III. Entropy is also insensitive to hardware phase offsets, which are discussed in the next paragraph. The analyses to evaluate the performance of different Doppler phase shift correction procedures are not discussed in this paper.

B. Hardware Relative Phase Offsets

In the case of POLDIRAD, phase offsets due to hardware configurations are considerable and must be known. One way of calibrating the scattering matrices is to select an area of light rain in the front of the observed event. Such target is supposed to have no backscatter differential phase shift due to Mie scattering, the cross-polar signals do not fall in the noise level, and propagation effects do not affect the signatures. The two cross-polar hardware offset phases can be estimated directly at zero lag as [2]

$$\hat{\Phi}^{h}_{\mathrm{cx\_hw}} = \arg\left[\sum_{n=1}^{N} S_{HH}[2n-1]\,(S_{VH}[2n-1])^*\right] \tag{12}$$

$$\hat{\Phi}^{\nu}_{\mathrm{cx\_hw}} = \arg\left[\sum_{n=1}^{N} S_{VV}[2n]\,(S_{HV}[2n])^*\right]. \tag{13}$$

For the estimation of the copolar hardware offset phase, the first Doppler phase shift correction must be performed with one of the procedures illustrated in the previous paragraph. For the calibration area, it is desirable that the difference between $\hat{\Phi}^{HHHH}_{\mathrm{DOPPLER}}$ and $\hat{\Phi}^{VVVV}_{\mathrm{DOPPLER}}$ be small, so that the one pulse lag estimator can be used to estimate the copolar hardware phase offset

$$\Psi_{\mathrm{DP}} = \Phi^{HHVV}_{\mathrm{DOPPLER}} + \Phi_{\mathrm{co\_hw}} \tag{14}$$

$$\hat{\Phi}_{\mathrm{co\_hw}} = \frac{1}{2}(\widetilde{\Psi}_2 - \widetilde{\Psi}_1). \tag{15}$$

After estimating the hardware offset phases for every bin, these are averaged over the calibration area.

III. Theory

A. Degree of Polarization

Measurements done with a dual-polarization coherent receiver can be considered as samples of a random Jones vector of the form

$$E(t) = \begin{bmatrix} E_1(t) \\ E_2(t) \end{bmatrix} = \begin{bmatrix} |E_1(t)|\, e^{i\varphi_1(t)} \\ |E_2(t)|\, e^{i\varphi_2(t)} \end{bmatrix}. \tag{16}$$

The covariance of a random Jones vector (Wolf's coherence matrix J) and the degree of polarization p read [5], [19]

$$\mathrm{Cov}(E) = J = \left\langle E \otimes E^{+} \right\rangle \tag{17}$$

$$p = \sqrt{1 - \frac{4\det(J)}{(\mathrm{trace}(J))^2}} = \frac{\lambda_1 - \lambda_2}{\lambda_1 + \lambda_2}. \tag{18}$$

The symbol $\otimes$ indicates external product. As λ_1 and λ_2 are Wolf's coherence matrix eigenvalues, the degree of polarization p is a basis invariant quantity, and as such does not depend on the orthogonal pair of polarimetric channels chosen to sample the backscattered wave. This fact is implicit in the unitary transformation U, corresponding to a polarization basis transformation for Wolf's coherence matrix

$$J' = UJU^{-1}. \tag{19}$$

For a coherent target, the backscattered wave is totally polarized, regardless of the transmit-polarization state. For an incoherent target, the degree of polarization of the backscattered wave does, in general, depend on the polarization state of the transmitted wave. Such function, which may be named as depolarization response, can be plotted either on the Poincaré sphere or with the help of surface plots, and it can be indicated with $p(\chi, \psi)$, where χ and ψ are the ellipticity and orientation angles of the transmitted polarization state, respectively. Even though straightforward, it is helpful to observe that the depolarization response of a coherent target is constant and equal to one. Furthermore, it is useful to define the minimal (maximal) degree of polarization as the degree of polarization corresponding to the minima (maxima) of the depolarization response function and indicate it with $p_{\mathrm{MIN}}(p_{\mathrm{MAX}})$. Other subscripts can be used to refer to the degree of polarization corresponding to a given transmit state: p_{RHC}, p_{LHC}, and p_C can be used to refer to right-hand circular, left-hand circular, or circular (with no further specification) polarization transmit states, respectively; p_{+45}, p_{-45}, and p_{45} can be used to refer to $+45^\circ$ linear, -45° linear, or slant (with no further specification) polarization transmit states, respectively; and p_H and p_V can be used to refer to horizontal and vertical polarization transmit states, respectively.

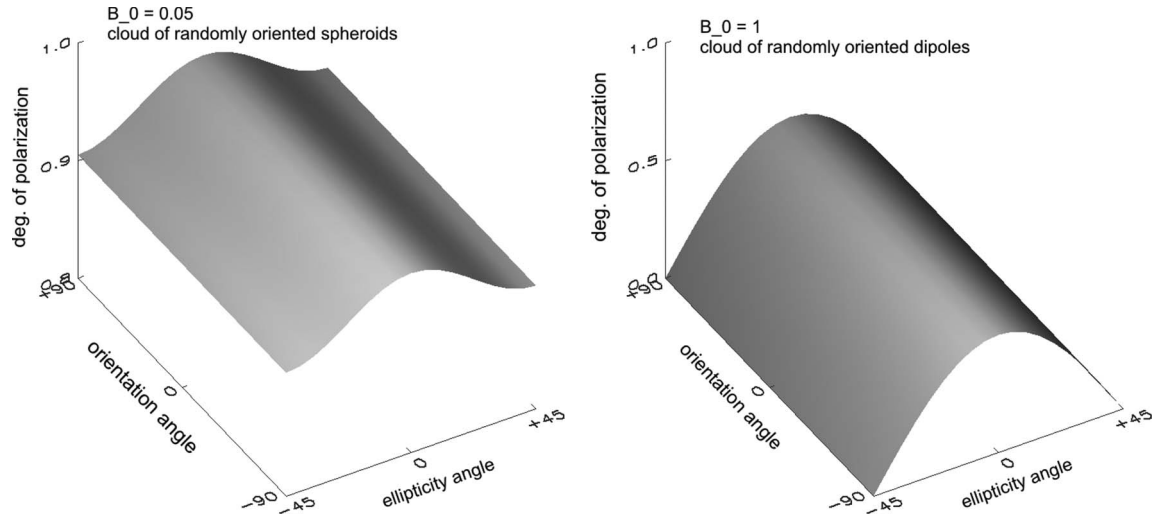

Fig. 2. (Left) Depolarization response for a cloud of randomly oriented slightly oblate spheroids ($B_0 = 0.05$). (Right) Depolarization response for a cloud of randomly oriented dipoles ($B_0 = 1$). Note the different scales on z-axis, which are [0.0–1.0] for the dipoles and [0.8–1.0] for the spheroids. For a cloud of spheres ($B_0 = 0.0$), the depolarization response is constant and equal to one.

A convenient way for the evaluation of the depolarization response of incoherent targets is provided by the Kennaugh matrix

$$K = \frac{1}{2}\left\langle Q^{\mathrm{T}}\left[S \otimes S^{*}\right] Q\right\rangle \tag{20}$$

$$Q = \begin{bmatrix} 1 & 1 & 0 & 0 \\ 0 & 0 & 1 & -j \\ 0 & 0 & 1 & +j \\ 1 & -1 & 0 & 0 \end{bmatrix}$$

$$S = \begin{bmatrix} S_{11} & S_x \\ S_x & S_{22} \end{bmatrix}.$$

The parameterizations of the Kennaugh matrix in terms of S matrix elements or Huynen parameters can be found in [17] and [20].

In the following, we analyze the depolarization response for the two cases of interest for weather radar applications: isotropic targets (differential reflectivity close to 0 dB; examples might be graupel, hail, or dry snow) and anisotropic targets (positive differential reflectivity, like rain or rain/small hail mixtures).

1) Isotropic Targets: A simple model for isotropic weather targets can be thought of as a cloud of randomly oriented spheroids. Considering the Huynen parameters [17], a simple way to compute the degree of polarization as a function of the transmitted polarization state is obtained by means of the Kennaugh matrix in

$$K_{\mathrm{iso}} = \begin{bmatrix} 1+B_0 & 0 & 0 & 0 \\ 0 & 1 & 0 & 0 \\ 0 & 0 & 1 & 0 \\ 0 & 0 & 0 & -1+B_0 \end{bmatrix}. \tag{21}$$

B_0 ranges between zero and one, depending if the spheroids are spheres ($B_0 = 0$) or dipoles ($B_0 = 1$). Simple algebra yields the following expression for the depolarization response for a cloud of randomly oriented spheroids:

$$p(\chi) = \frac{\sqrt{\cos^2(2\chi) + (1-B_0)^2 \sin^2(2\chi)}}{1+B_0}. \tag{22}$$

Here, χ is the ellipticity angle, and B_0 is the generator of target structure. The aforementioned expression shows that, for an isotropic target, the degree of polarization attains its minimal values at the poles of the Poincaré sphere (circular polarization transmit) and the maximal values at the equator (linear polarization transmit) (Fig. 2). Furthermore, if we consider the quantity $1-p$, the relation between the minimum and the maximum is a simple 3-dB difference

$$1 - p_{\mathrm{MIN}} = \frac{2B_0}{1+B_0} \qquad 1 - p_{\mathrm{MAX}} = \frac{B_0}{1+B_0}. \tag{23}$$

The depolarization response of an isotropic target shows a number of symmetries, namely, the invariance with respect to orientation angle and the handedness of the transmitted polarization state.

It is worth noting that the depolarization responses corresponding to $B_0 = 0$ and $B_0 = 2$ are constant and equal to one and 1/3, respectively. The first case could be realized by a cloud of spheres, whereas the second could be obtained by an admixture of randomly oriented dipoles and a suitable balance of right and left helices [33].

2) Anisotropic Targets: A Kennaugh matrix that can qualitatively illustrate the depolarization response pattern for rain can be constructed as a cloud of spheres plus a cloud of oblate horizontally oriented spheroids. The two Kennaugh matrices that come in the sum can be computed from the respective scattering matrices with the help of (20).

As an example, from the following scattering matrices:

$$S_{\mathrm{sphere}} = \begin{bmatrix} 1 & 0 \\ 0 & 1 \end{bmatrix} \qquad S_{\mathrm{oblate}} = \begin{bmatrix} 1 & 0 \\ 0 & 0.5 \end{bmatrix} \tag{24}$$

the plot shown in Fig. 3 can be obtained.

The depolarization response of this bimodal distribution has a different pattern than the isotropic case: The degree of polarization attains its minimal values on the circular/slant circle of the Poincaré sphere (the great circle containing the poles and $+/-45^{\circ}$ linear polarization) and its maximal values (one) at horizontal and vertical linear transmit states (Fig. 3). In the case of rain or rain/hail mixtures, the degree of polarization

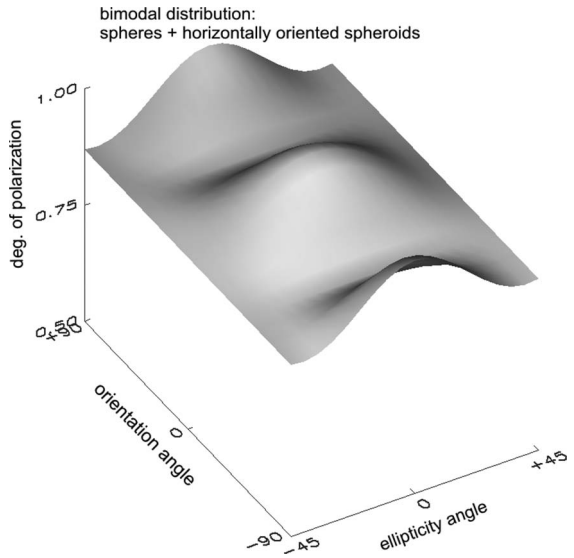

Fig. 3. Depolarization response for anisotropic targets. The corresponding Kennaugh matrix is synthesized as a cloud of spheres plus a cloud of horizontally oriented spheroids (bimodal distribution). The corresponding S matrices are reported in (24).

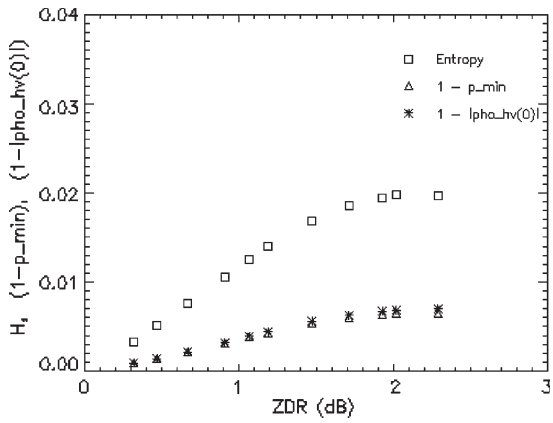

Fig. 4. Simulation results for a cloud of noncanted raindrops with exponential drop size distribution (Marshall–Palmer). The plots reported in the graph correspond to (squares) entropy, (triangles) one minus the minimal degree of polarization, and (asterisks) one minus the copolar correlation coefficient. The covariance matrix used for the simulation is shown in (25). Note the almost identical values assumed by p_{MIN} and $|\rho_{h\nu}(0)|$.

at horizontal or vertical transmit states is the least sensitive to depolarization effects.

For the case of rain, the values of entropy, copolar correlation coefficient, and minimal degree of polarization were evaluated also for a more realistic case, namely, for a Marshall–Palmer drop size distribution.

The covariance matrix (containing equivalent information to the Kennaugh matrix) was computed for a cloud of noncanted raindrops, using the Rayleigh approximation. The formulas needed to evaluate the matrix elements can be found in [5], [21], and [22], as shown in (25) given at the bottom of the page.

The Marshall–Palmer drop size distribution (Fig. 4) is an exponential distribution of the form

$$\begin{aligned} N(D) &= N_0 \cdot e^{-\Lambda D} \\ N_0 &= 8000\ \mathrm{m}^{-3} \cdot \mathrm{mm}^{-1} \\ \Lambda &= 4.1 \cdot R^{-0.21} \end{aligned} \tag{26}$$

where R is the rain rate in mm/h.

After the evaluation of the copolar correlation coefficient, the covariance matrix was either diagonalized to evaluate the scattering entropy or rotated to circular polarization to evaluate the minimal degree of polarization. The simulation yields numerical values for H, $(1 - p_{\mathrm{MIN}})$, and $(1 - |\rho_{h\nu}(0)|)$ and shows how these quantities are affected by raindrop oblateness dispersion. Note that, even though not included in the model, Mie scattering might also contribute to the numerical value of the variables in question.

On the other hand, p_H and p_V are identically zero for a cloud of noncanted raindrops, and as a consequence, these variables are expected to enhance the contrast between rain and clutter or between rain and nonweather targets in a way that is unique.

Ultimately, it is helpful to remind some theoretical relationships between the minimal degree of polarization and the copolar correlation coefficient [19].

Under the assumption of a diagonal scattering matrix (oblate noncanted raindrop) acting on slant polarization

$$\begin{bmatrix} S_{HH} \\ S_{VV} \end{bmatrix} = \begin{bmatrix} S_{HH} & 0 \\ 0 & S_{VV} \end{bmatrix} \begin{bmatrix} 1 \\ 1 \end{bmatrix} \tag{27}$$

simple algebra leads to the following relationship between the degree of polarization at slant send and the copolar correlation coefficient:

$$\left(1 - p_{45}^2\right) = \left[\frac{2|S_{HH}||S_{VV}|}{|S_{HH}|^2 + |S_{VV}|^2}\right]^2 \left(1 - |\rho_{h\nu}(0)|^2\right). \tag{28}$$

Almost identical algebra yields the same result for the degree of polarization at circular send (p_C).

All these considerations suggest a similar behavior for p_{45}, p_C, and $|\rho_{h\nu}(0)|$ when rain is illuminated. There is, however, an important difference. Contrary to p_C, which is canting independent, both quantities appearing in round brackets in (28) show a linear dependence on canting angle.

3) Propagation: Regardless of the polarization state of the transmitted wave, the degree of polarization is independent from polarization-independent attenuation, as this simply appears as a scalar factor multiplying Wolf's coherence matrix.

If the transmit state lies on the circular/slant circle of the Poincaré sphere, differential propagation phase (Φ_{DP}) occurring from the antenna to the target is responsible for a migration of the polarization state of the forward propagating wave along

$$C = \begin{bmatrix} \int S_{HH}(D) \cdot S_{HH}^*(D) \cdot N(D)\, dD & 0 & \int S_{HH}(D) \cdot S_{VV}^*(D) \cdot N(D)\, dD \\ 0 & 0 & 0 \\ \int S_{VV}(D) \cdot S_{HH}^*(D) \cdot N(D)\, dD & 0 & \int S_{VV}(D) \cdot S_{VV}^*(D) \cdot N(D)\, dD \end{bmatrix} \tag{25}$$

this circle. If the illuminated targets have a depolarization response as in Fig. 3 (noncanted rain), no bias occurs as the $\Phi_{\rm DP}$-induced migration displaces the polarization state of the propagating wave along a minimal circle. If the illuminated targets are isotropic, the degree of polarization is dependent upon the one-way differential phase shift (from the antenna to the target). As shown in (23), the bias can be up to 3 dB; however, because the differential propagation phase can be measured independently, it is possible to correct for this effect by means of (22). Ultimately, with the help of (29), the generator of target structure of isotropic targets can be estimated

$$p = \frac{\sqrt{\cos^2(\Phi_{\rm DP}) + (1 - B_0)^2 \sin^2(\Phi_{\rm DP})}}{1 + B_0}. \tag{29}$$

At H or V send, the differential propagation phase does not change the polarization state of the forward propagating wave, and as a consequence, the degrees of polarization corresponding to these transmit states are to a first order $\Phi_{\rm DP}$ independent.

Differential phase shifts occurring after the scattering, namely, from the target to the antenna, do not further affect the degree of polarization of the backscattered wave. This fact is again encapsulated in (19) as nonattenuating propagation effects in the atmosphere map to unitary transformations.

B. Entropy

The terms of a monostatic scattering matrix using the backscatter alignment convention can be arranged in a target feature vector [5]

$$\begin{bmatrix} S_{HH} & S_{HV} \\ S_{HV} & S_{VV} \end{bmatrix} \rightarrow \begin{bmatrix} S_{HH} \\ \sqrt{2} S_{HV} \\ S_{VV} \end{bmatrix} = \underline{\Omega}_i. \tag{30}$$

After averaging over a given number of samples, which is supposed to be the representative of the same weather target (wide-sense stationarity is assumed), the covariance matrix can be obtained

$$[C] = \sum_i \underline{\Omega}_i \cdot \underline{\Omega}_i^+ = \begin{bmatrix} \langle |S_{HH}|^2 \rangle & \sqrt{2} \langle S_{HH} S_{HV}^* \rangle & \langle S_{HH} S_{VV}^* \rangle \\ \sqrt{2} \langle S_{HV} S_{HH}^* \rangle & 2 \langle |S_{HV}|^2 \rangle & \sqrt{2} \langle S_{HV} S_{VV}^* \rangle \\ \langle S_{VV} S_{HH}^* \rangle & \sqrt{2} \langle S_{VV} S_{HV}^* \rangle & \langle |S_{VV}|^2 \rangle \end{bmatrix}. \tag{31}$$

The covariance matrix C is always Hermitian positive semidefinite and, upon diagonalization, yields nonnegative real eigenvalues. This similarity transformation is such that an incoherent scattering process is decomposed into a convex sum of three rank-one covariance matrices. The columns of the unitary matrix U_3 contain the orthonormal eigenvectors (u_i) that generate the rank-one covariance matrices [8], [9]

$$[C] = [U_3] \begin{bmatrix} \lambda_1 & 0 & 0 \\ 0 & \lambda_2 & 0 \\ 0 & 0 & \lambda_3 \end{bmatrix} [U_3]^+, \qquad \lambda_1 \geq \lambda_2 \geq \lambda_3 \geq 0$$

$$[U_3] = [\, u_1 \quad u_2 \quad u_3 \,]$$

$$\langle [C] \rangle = \lambda_1 u_1 u_1^* + \lambda_2 u_2 u_2^* + \lambda_3 u_3 u_3^*. \tag{32}$$

Entropy is defined as follows [7]–[9], where P_i is the relative probability of each principal component

$$P_i = \frac{\lambda_i}{\sum \lambda_i}, \qquad 0 \leq P_i \leq 1 \tag{33}$$

$$H = -\sum_{i=1}^{3} P_i \log_3(P_i), \qquad 0 \leq H \leq 1. \tag{34}$$

Hence, entropy is a scalar quantity relating to the heterogeneity of statistically independent degrees of freedom existing in the scattering population. Entropy is sensitive to the heterogeneity of scattering matrices coming from the formation of the covariance matrix. Wolf's coherence matrix is sensitive only to one half of the information contained in the covariance matrix, and as such, its capability of capturing polarimetric heterogeneity is reduced. Because of the underlying mathematical structure, entropy can be regarded as the optimal indicator of polarimetric heterogeneity.

1) Propagation: Propagation through a medium can be described by a matrix T acting on a covariance matrix C (cross indicates adjoint) [23]

$$C' = TCT^+. \tag{35}$$

In the case of T being unitary, (35) reduces to a similarity transformation. Such transformation set contains (in the strict sense) the set of polarization basis change, which, in turn, contains the set of rotations around the radar line of sight [8]. Because the eigenvalue problem is intrinsically invariant under unitary transformations, two observations can be made. The first is that, because of roll invariance, whenever an anisotropic cloud of hydrometeors is illuminated, entropy is not dependent on the mean canting angle (insofar as only a rotation of the symmetry axis of the target occurs, and the orientation distribution keeps unaltered). The second is that, because unitarity corresponds to energy conservation, propagation phenomena associated with nonattenuating media with different electrical lengths at different polarizations do not affect entropy (in particular, entropy is not affected by differential propagation phase). More specifically, the matrix T modeling propagation through a nonattenuating medium is an element of a representation of the rotation group $SO(3)$, which is a subgroup of $U(3)$. Nonattenuating propagation effects in the atmosphere map to $SL(2, C)$ over $SU(2)$, and the corresponding group representation is $SO(3, C)$, which is isomorphic to the Lorentz group $SO(3, 1)$. Nonattenuating propagation effects map to a smaller set than $U(3)$ because the latter contains power-preserving transformations that cannot physically occur in the atmosphere.

Furthermore, because entropy is explicitly normalized with respect to power, it is unaffected by polarization-independent attenuation (but it is affected by differential attenuation). Entropy is an amplitude invariant scalar like $Z_{\rm DR}$ and LDR, but unlike the latter, it has the property of being canting independent.

IV. Data Analysis

Entropy and the degree of polarization are evaluated with the data collected by the DLR C-band POLDIRAD. The radar was operated in fully polarimetric mode, transmitting alternating

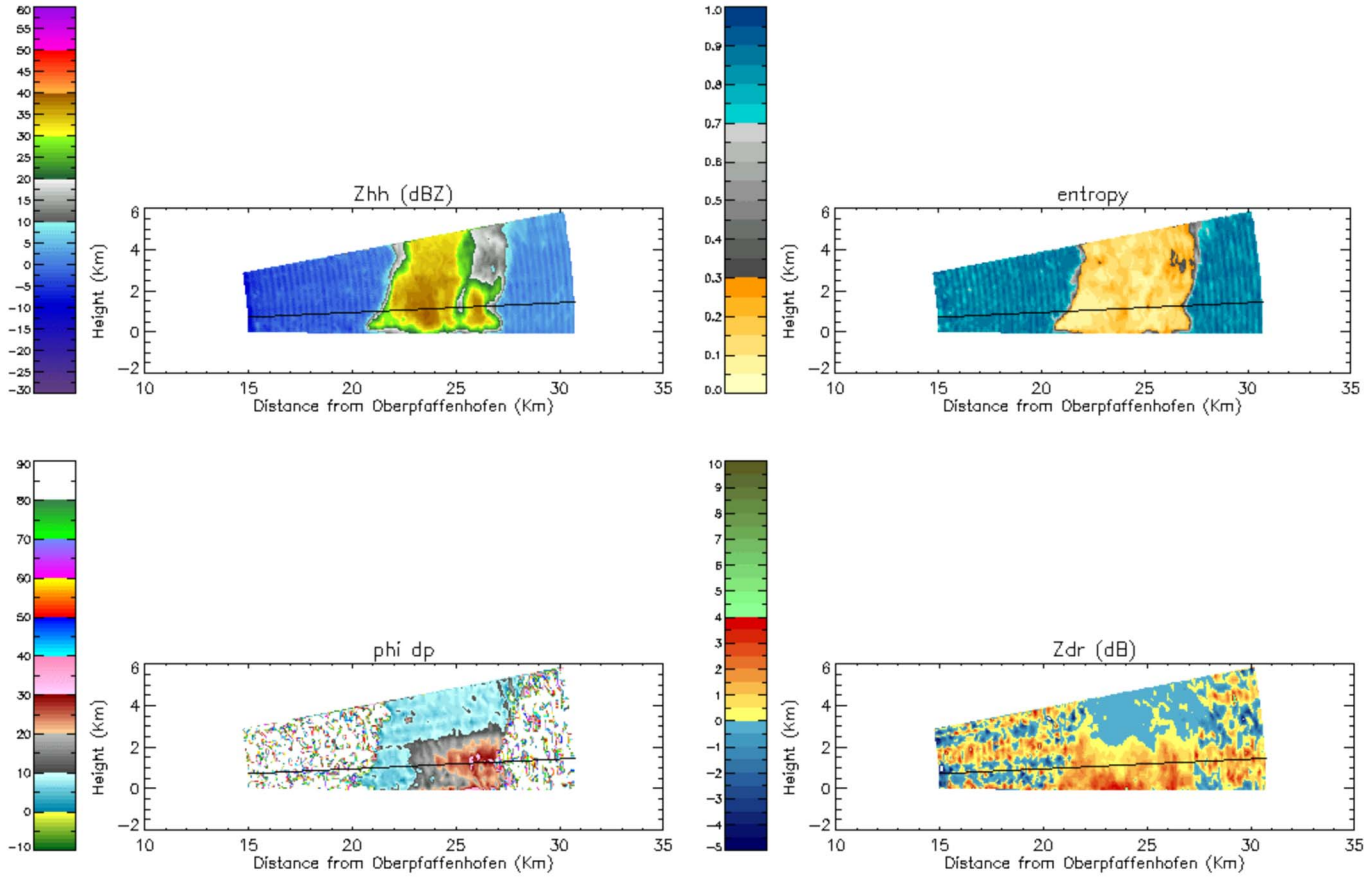

Fig. 5. Convective event, RHI images. (Upper left) Reflectivity (Z_{HH}; in dBZ). (Upper right) Entropy (H). (Lower left) Copolar phase ($\Phi_{\rm DP}$; Doppler shift corrected). (Lower right) Differential reflectivity ($Z_{\rm DR}$; in decibels). The black ray is chosen for the analysis of entropy, degree of polarization, and copolar correlation coefficient when anisotropic targets (rain or rain/small-hail mixtures) are illuminated. The corresponding rayplots are shown in Fig. 6.

horizontal and vertical polarization states and receiving the co- and cross-polar components of the backscattered signal, thus allowing estimation of complete scattering matrices at H/V polarization basis. The convective event (June) was observed at 16.00 local time with pulse repetition frequency PRF $= 1200$ Hz and pulsewidth $\tau = 1$ μs. The stratiform event (November) was taken at 13.05 local time and 272° azimuth with PRF $= 800$ Hz and $\tau = 1$ μs. Aside from being fully polarimetric, these data sets have the desirable advantage of range height indicator (RHI) scan mode. RHIs are obtained by scanning in elevation for a fixed azimuth direction, and the resulting image appears as a vertical section of the illuminated event, allowing analysis of rayplots in context.

A. Convective Event

The first case study presents a convective event characterized by two cores located at approximately 24 and 26 km away from the radar. $\Phi_{\rm DP}$ and $Z_{\rm DR}$ signatures guarantee a major presence of rain in the lowest 2–2.5 km. In correspondence to the center of the first core (24 km), a mixture of rain and frozen irregularly shaped hydrometeors is probably responsible for higher values of Z_{HH}, H, and $1-p$. Accordingly, $Z_{\rm DR}$ assumes smaller values of around 0.5 dB.

After the evaluation of standard radar meteorological variables, a ray passing through the core of the storm (highlighted in black in Fig. 5) was chosen for the rayplots shown in Fig. 6. This case study focuses on anisotropic weather targets (rain or rain/small-hail mixture) and aims at the following:

1) confronting the sensitivity to depolarization from the rain of the following variables: entropy (H), the degree of polarization at horizontal send (p_H), the degree of polarization at vertical send (p_V), the degree of polarization at circular send[1] (p_C), the degree of polarization at slant send (p_{45}), and copolar correlation coefficient ($|\rho_{h\nu}(0)|$);
2) identifying the scattering phenomena that are responsible for the depolarization from rain and their impact on the variables under consideration.

As shown in Fig. 6, the degree of polarization at horizontal send (p_H) behaves very similarly to the degree of polarization at vertical send (p_V). The same happens for the pair (p_{+45}) and (p_{-45}) and the pair $p_{\rm RHC}$ and $p_{\rm LHC}$ (graphs not reported for compactness). Furthermore, p_{45} behaves very similarly to p_C, and both variables take on smaller values than p_H or p_V. These observations are in qualitative accordance with the theoretical description provided by the depolarization response for anisotropic weather targets provided in Section III.

The condition for a cloud of horizontally oriented spheroids to show a minimal depolarization response on the circular/slant

[1]The degree of polarization at circular and slant send was evaluated after performing unitary transformations. The data were corrected for the Doppler phase shift but not for the differential propagation phase.

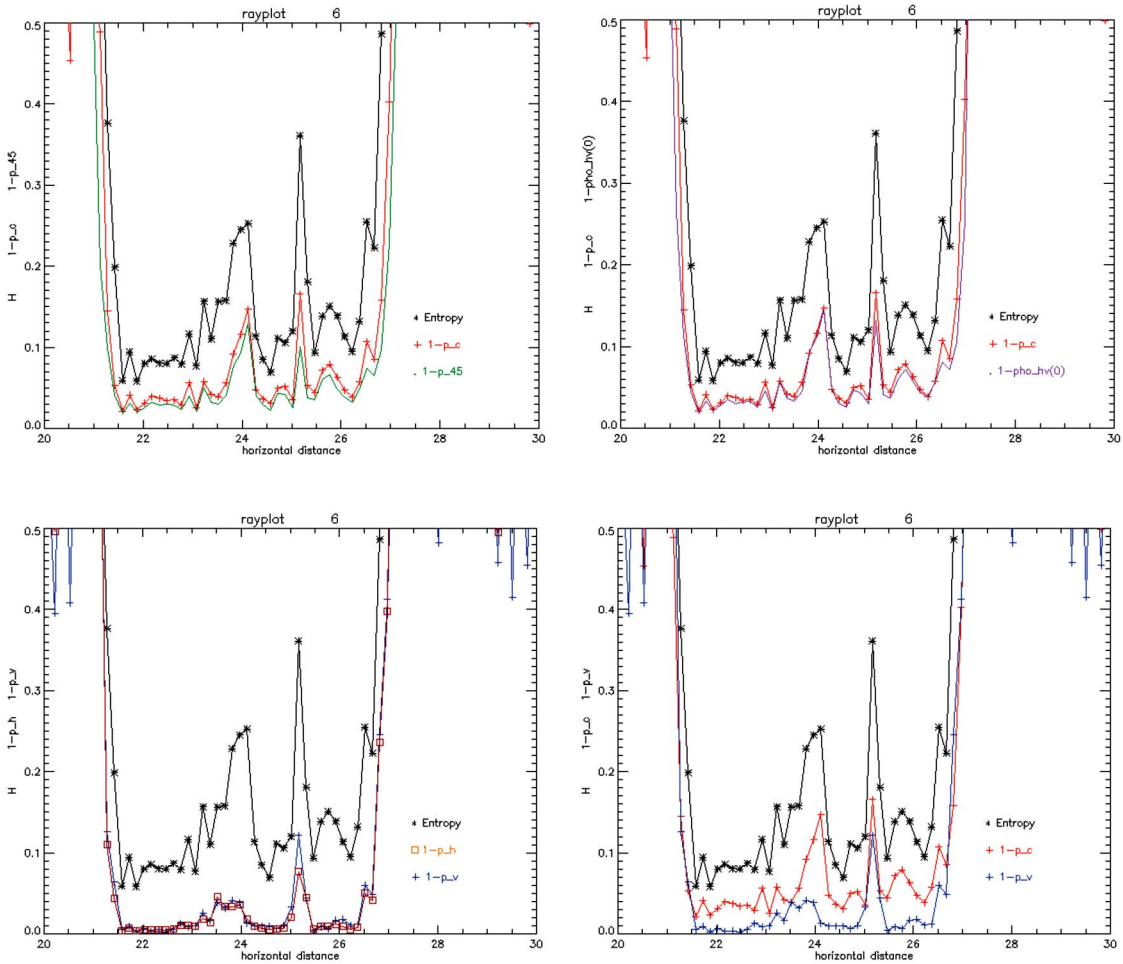

Fig. 6. Rayplots corresponding to the ray in black in Fig. 5. The top plot on all of the four graphs is the entropy (H; in black). In the upper left graph are two minimal degrees of polarization, namely, at circular transmit (p_C; in red) and 45° linear transmit (p_{45}; in green). In the lower left graph are the two maximal degrees of polarization, which are at horizontal transmit (p_H; in orange) and vertical transmit (p_V; in blue). In the upper right graph are the minimal degree of polarization (at circular transmit p_C; in red) and the copolar correlation coefficient (in violet). In the lower right graph are the minimal degree of polarization (at circular transmit p_C; in red) and the maximal degree of polarization (at vertical transmit p_V; in blue). The images show the different sensitivities of the minimal and maximal degrees of polarization to the depolarizing properties of rain. The copolar correlation coefficient performs very similarly to the minimal degree of polarization, and its sensitivity appears comparable to entropy. The maximal degree of polarization (at horizontal or vertical transmit) shows decreased sensitivity to depolarization effects from anisotropic targets.

circle is to have an axis-ratio distribution. In the limit, a simple incoherent target showing such behavior can be constructed as a cloud of spheres plus a cloud of the same axis-ratio horizontally oriented spheroids, namely, the bimodal distribution used in Section III. The dispersion in axis ratios corresponds to variability in scattering mechanisms, which is naturally perceived by entropy but not necessarily by the degree of polarization. Indeed, if the transmit polarization is horizontal, every scatterer (regardless of its axis ratio) responds with a horizontally polarized wave, producing no depolarization on backscatter. For slant transmit on the other hand, (but in theory, this holds for any transmit-polarization state other than horizontal or vertical) every scatterer responds with a polarization state that is dependent on its axis ratio, thus producing depolarization on backscatter.

The aforementioned observations suggest that, among all possible degrees of polarization, the minimal is the most effective in capturing depolarization effects, and as a consequence, its performance is expected to be comparable to entropy. The graphs in Fig. 6 confirm that H and p_{MIN} (although assuming different numerical values) have similar patterns. Fig. 6 also shows that, as expected from the theoretical results in Section III, the copolar correlation coefficient and the minimal degree of polarization take on almost identical values. The maximal degrees of polarization (p_H and p_V) show, on the other hand, decreased sensitivity to depolarization from rain.

Regardless of the different sensitivities, all these variables (p_{MIN}, p_{MAX}, $|\rho_{h\nu}(0)|$, and H) are capable of distinguishing between rain (22–23 km) and mixtures of rain and small-hail (24 km).

As far as propagation is concerned, the theory and experimental data are in agreement and confirm that H, p_H, and p_V are not sensitively affected by differential propagation phase which, in the far range, attains values of 30°.

At 22–23-km distance, radar cells are presumably filled with rain, and the signatures are not affected by the differential propagation phase. The degree of polarization at horizontal or vertical send should be identically zero for every rain rate, and in this case, experimental data do agree with the theory rather satisfactorily (p_H and p_V take on low values, which are less than 0.01). A discrepancy occurs when confronting experimental and simulated values of H, p_C, p_{45}, and $|\rho_{h\nu}(0)|$.

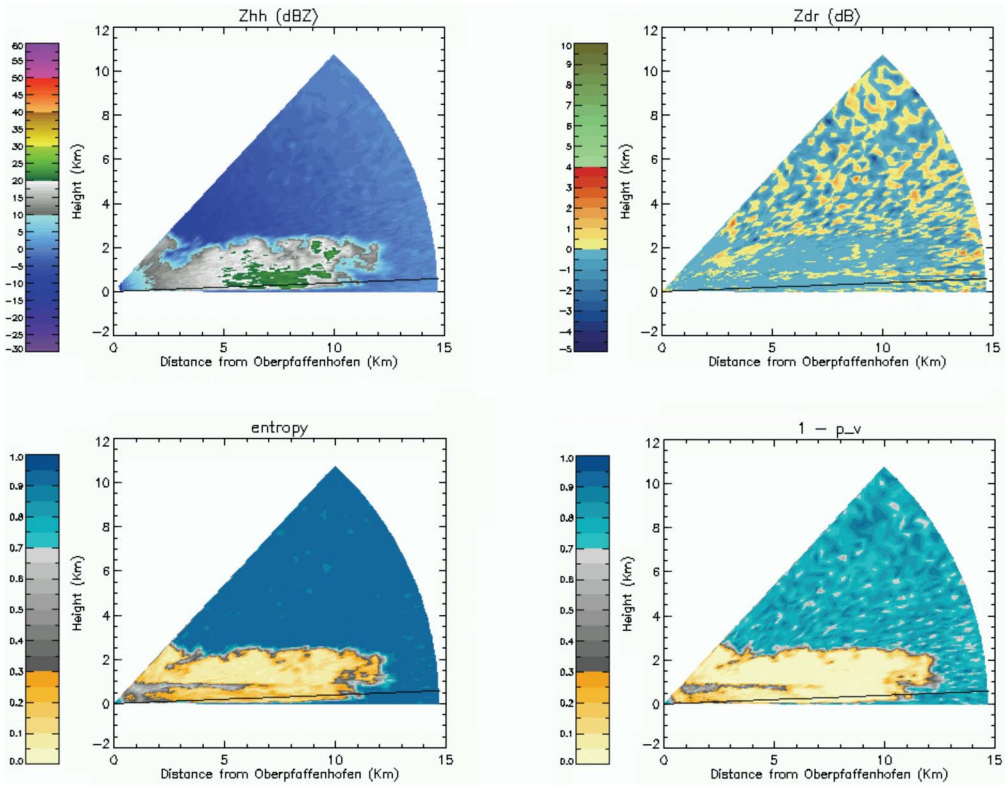

Fig. 7. Stratiform event, RHI images. Upper left image is reflectivity (Z_{HH}; in dBZ), upper right is differential reflectivity (Z_{DR}; in decibels), lower left is entropy, and lower right is the degree of polarization at vertical transmit ($1 - p_{\mathrm{v}}$). The entropy and the degree of polarization are capable of detecting the melting band, which are clearly visible in the images with values that can exceed 0.3 for both variables. Ray in black is number 8; corresponding elevation is 2.26°.

In the area under consideration, where differential reflectivity takes on values of 1–2 dB, the measured values for p_C and $|\rho_{h\nu}(0)|$ are around 0.03, whereas simulated values are around 0.005.

In this paper, it is possible to compare parameters that are normally associated with different transmission states through the ability to synthesize full scattering matrices. This allows us to rule out some of the possible mechanisms of depolarization, which can be expected to occur to a similar degree in either modes. As the polarization basis transformations involved in the processing are linear, noise should, in principle, affect equally p_H or p_V and p_C or p_{45}. The effect of noise on the degree of polarization at horizontal or vertical send is small, and as a consequence, it does not seem reasonable to indicate it as the responsible for the observed discrepancy between experimental and simulated results for p_C, p_{45}, $|\rho_{h\nu}(0)|$, and H.

Aside from a variability of axis ratio induced by the drop size distribution (modeled in the simulation), factors that affect differentially p_{MAX} on one side and $|\rho_{h\nu}(0)|$ and p_{MIN} on the other are drop oscillations and Mie scattering.

Our simulation considers an axis-ratio variability given by raindrops in their equilibrium shape. However, what is actually perceived by the radar variables is the "instantaneous" axis-ratio distribution. Axisymmetric drop oscillations are responsible for the enhancement of "instantaneous" axis-ratio variability, and it might be a factor contributing to the discrepancy between data and numerical results.

At C-band, scattering from large raindrops can deviate from the Rayleigh model assumed in the simulation. According to the Mie theory, every spheroid responds with a backscatter differential phase that is dependent on its size. If the transmit polarization lies on the circular/slant circle (p_C or p_{45}), this phenomenon might be responsible for a further dispersion in the polarization states backscattered by the target. In this case, $|\rho_{h\nu}(0)|$ is also affected. A simulation for $|\rho_{h\nu}(0)|$ at C-band, considering Mie scattering and a Gaussian distribution of canting angles with a mean of 0° and a standard deviation of 7°, is reported in the literature [5]. For a Z_{DR} of around 1–2 dB, it yields values for $1 - |\rho_{h\nu}(0)|$ of around 0.02. The inclusion of Mie scattering appears to provide numerical results that match more satisfactorily with the experimental data (0.03).

The analysis of this case study suggests that drop size distribution, drop oscillations, and Mie scattering do not affect p_H and p_V but have an impact on the numerical values of H, p_{45}, p_C, and $|\rho_{h\nu}(0)|$. Furthermore, in the presence of all these scattering phenomena, the numerical values of p_{45}, p_C, and $|\rho_{h\nu}(0)|$ are almost identical. The differences between these variables $(p_C - p_{45})$ or $(p_C - |\rho_{h\nu}(0)|)$ might be indicators of canting effects. Further work should be addressed at the experimental and theoretical investigations of these differences because they could be available to weather radars operating in hybrid mode.[2]

B. Stratiform Event

The second data set relates to a stratiform event with a clearly visible melting band located 1 km above the ground (Fig. 7).

[2]In presence of canting the copolar correlation coefficient measured at hybrid mode differs from the copolar correlation coefficient measured at alternate H/V. The latter is the one being considered in this paper.

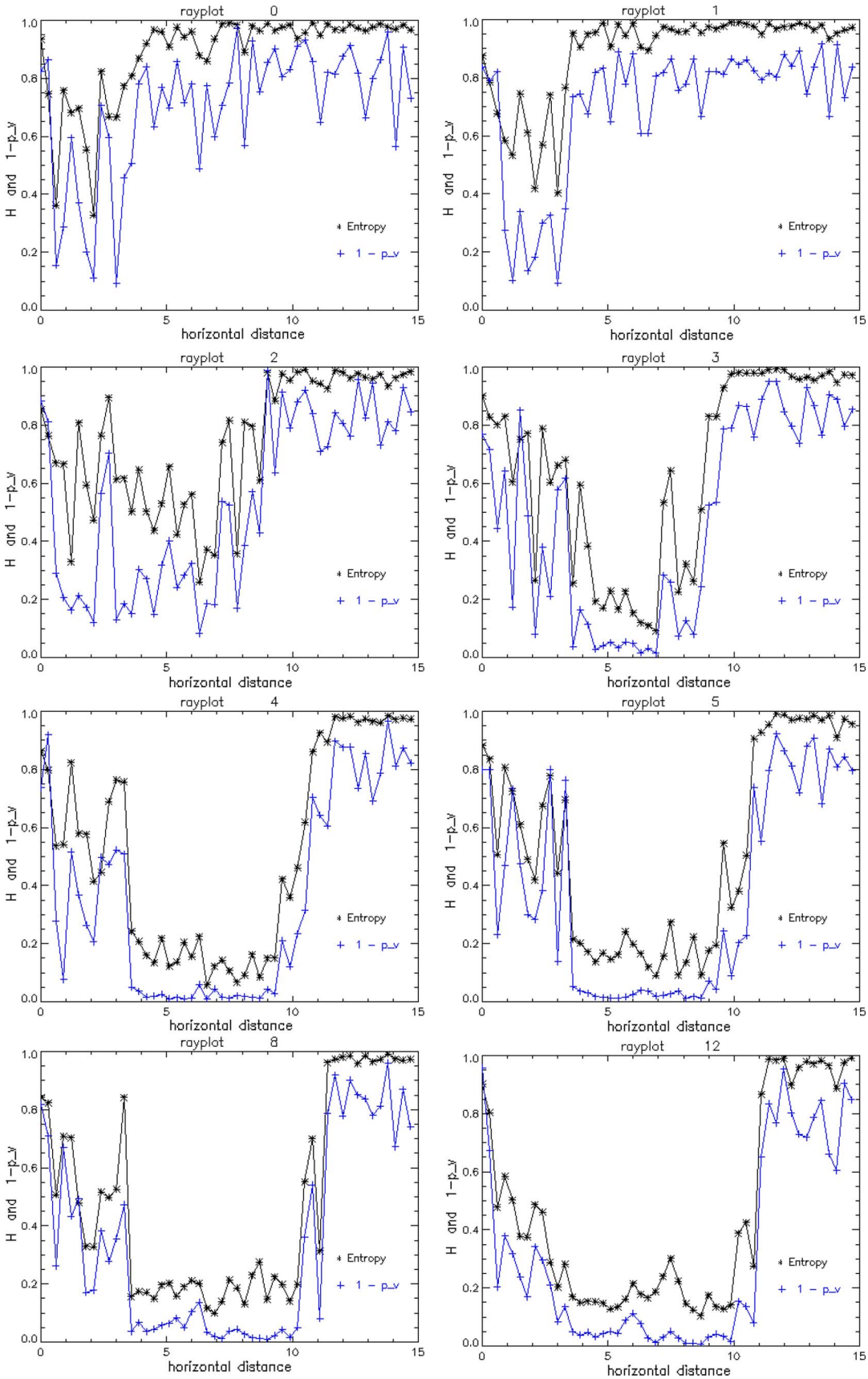

Fig. 8. The rayplots show the different contributions of clutter for progressively increasing elevations. Rayplots are labeled with the number in the RHI data set ranging from the lowest ray (rayplot 0; elevation angle of -0.30°) to higher rays (rayplot 12; elevation of 3.04°). Rayplot 8 corresponds to the ray in black in Fig. 7. The entropy and the degree of polarization are sensitive indicators of the presence of clutter.

Aside from standard radar meteorological variables, H, p_H, and p_V were evaluated to conduct a phenomenological analysis of their behavior in the presence of stratiform precipitation and ground clutter. Even though worked out from experimental data, the numerical values given in the following are indicative and not meant to fully characterize the hydrometeor classes they refer to. Further work is needed, for example, to evaluate membership functions for implementation in hydrometeor classification algorithms.

A visual analysis of the images shown in Fig. 7 suggests the presence of rain and dry snow below and above the melting band, respectively. H and p can detect wet snow (melting band) with values that can exceed 0.3, whereas rain and dry snow appear to be characterized by lower values. Typical values for rain are less than 0.1 for H and less than 0.01 for p_H and p_V.

Aside from enabling detection of the melting band, the relatively low depolarizing properties of rain and dry snow prompt the use of H and p for clutter detection, the latter being characterized by relevant cross-polarization on backscatter. In particular, when rain is present in the lower sections of the atmosphere, p_H or p_V enhances the contrast with clutter and should therefore perform better than H, p_C, p_{45}, or $|\rho_{h\nu}(0)|$. However, as the depolarizing properties of clutter are relevantly larger than rain, the use of more sensitive variables is not strictly excluded for this application.

In order to test sensitivity to ground clutter, a series of eight rays was chosen with the following elevation angles: -0.30°, -0.11°, 0.29°, 0.46°, 0.96°, 1.01°, 2.26°, and 3.04°. The corresponding rayplots are shown in Fig. 8 with labels 0, 1, 2, 3, 4, 5, 8, and 12. The labels correspond to the ray number in the RHI data set; rays 6, 7, 9, 10, and 11 are not shown for compactness. Ray 0 corresponds to the lowest elevation angle (-0.30°); ray 8 (elevation 2.26°) is plotted in black in Fig. 7.

In the first 3 km of every rayplot, the relatively high values of H and p suggest that the received signatures are dominated by switch leakage and side-lobe clutter.

Between 3 and 10 km from the radar, the graphs feature an interesting transition from high to low entropy patterns, as the ray elevation increases. This phenomenon is clearly due to the gradually changing contribution of high entropy clutter and low entropy weather targets to the backscattered signal. For this case study, the low entropy weather target is constituted by rain, but clutter detection should be feasible also when dry snow occupies the lowest layers of the atmosphere. It has to be noted that, even for ray 12 (elevation 3.04°), the values of H and p are higher than those normally expected for rain, indicating that the signatures are probably still contaminated with clutter. The presence of the latter becomes more relevant with decreasing elevation, as larger sections of the beam intercept the ground. In the limit, for rayplots 0 and 1 (corresponding to negative elevations of -0.30° and -0.11°, respectively), H and p assume values close to one, indicating that returns from the ground neatly dominate the signal.

Between 10 and 15 km, the main beam no longer impinges on weather targets, and no backscattered energy flows into the receiver. In this section of the rayplots, only hardware and external noise is detected, and due to the random nature of noise, H and p assume values close to one.

V. Conclusion

In this paper, we investigated the properties and evaluated the performance of depolarization-sensitive variables: entropy, degree of polarization, and copolar correlation coefficient. A preliminary theoretical analysis illustrates the properties of the degree of polarization at different transmit states. Analytical results are presented to illustrate the backscattering from isotropic and anisotropic weather targets and the sensitivity to propagation. Entropy, which is a quad-pol variable that is well known to the SAR-polarimetry community, is used to measure how well a particular degree of polarization can capture information. The copolar correlation coefficient, which is well known to the weather radar community, is used to evaluate the potential of entropy and the degree of polarization to add value to radar meteorological investigations. Fully polarimetric POLDIRAD data were used to evaluate entropy and, by means of unitary transformations, the degree of polarization for different transmit-polarization states.

The analytical and experimental results can be itemized as follows.

1) The capability of the degree of polarization of capturing depolarizing effects is dependent on transmit-polarization state and the type of incoherent target. The concept of depolarization response is introduced to illustrate this dependence. Furthermore, the impact of propagation effects has been analytically investigated and experimentally assessed. H, p_H, and p_V are insensitive to differential propagation phase, whereas p_{45} and p_C might, under given circumstances, be affected.
2) The capability of H, p_{45}, and p_C of distinguishing different hydrometeor types is similar to $|\rho_{h\nu}(0)|$. In particular, sensitivity to depolarization effects from rain is practically the same for $|\rho_{h\nu}(0)|$, p_{45}, and p_C, and they tend to assume the same numerical values. Differences might arise in the presence of canted raindrops. It is important to note that canting could affect differentially $|\rho_{h\nu}(0)|$ or p_{45} on one side and p_C on the other. Further work is needed to analyze the phenomenon, and the results might have relevance also from an operational perspective because $|\rho_{h\nu}(0)|$ and p_{45} or p_C are available to planned hybrid polarization operational weather radars.
3) It was analytically and experimentally shown that, when rain is illuminated, p_H and p_V have different properties with respect to H,p_{45}, p_C, or $|\rho_{h\nu}(0)|$. Namely, sensitivity to depolarization effects from raindrops is minimal. This feature prompts their use for the identification of nonweather targets like ground clutter or biological targets. Furthermore, the experimental data presented in this paper have demonstrated the capability of p_H and p_V to distinguish different hydrometeor types like rain, wet snow, and mixtures of rain and small/hail. The degree of polarization at horizontal transmit might bring complementary information to the set of radar variables available to dual-polarization coherent systems transmitting horizontal polarization, particularly, because in this case, $|\rho_{h\nu}(0)|$ is not available.

REFERENCES

[1] A. Schroth, M. Chandra, and P. F. Meischner, "A C-band coherent polarimetric radar for propagation and cloud physics research," *J. Atmos. Ocean. Technol.*, vol. 5, no. 6, pp. 803–822, Dec. 1988.

[2] V. Chandrasekar, J. Hubbert, V. N. Bringi, and P. F. Meischner, "Interpolation procedures to construct complete polarimetric signatures of distributed targets," *Proc. SPIE*, vol. 1748, pp. 200–212, 1992.

[3] E. A. Mueller, "Calculation procedure for differential propagation phase shift," in *Proc. 22nd Conf. Radar Meteorol. Preprints*, Zuerich, Switzerland, 1984, pp. 397–399.

[4] J. D. A. G. Kingsbury and Y. M. M. Antar, "Radar partially-polarized backscatter description algorithms and applications," in *Proc. IGARSS*, Houston, TX, 1992, pp. 74–76.

[5] V. N. Bringi and V. Chandrasekhar, *Polarimetric Doppler Weather Radar. Principles and Applications*. Cambridge, U.K.: Cambridge Univ. Press, 2001.

[6] R. J. Doviak and D. S. Zrnic, *Doppler Radar and Weather Observations*, 2nd ed. San Diego, CA: Academic, 1993.

[7] S. R. Cloude and E. Pottier, "Concept of polarization entropy in optical scattering," *Opt. Eng.*, vol. 34, no. 6, pp. 1599–1610, Jun. 1995.

[8] S. R. Cloude and E. Pottier, "A review of target decomposition theorems in radar polarimetry," *IEEE Trans. Geosci. Remote Sens.*, vol. 34, no. 2, pp. 498–518, Mar. 1996.

[9] S. R. Cloude and E. Pottier, "An entropy based classification scheme for land applications of polarimetric SAR," *IEEE Trans. Geosci. Remote Sens.*, vol. 35, no. 1, pp. 68–78, Jan. 1997.

[10] S. R. Cloude, J. Fortuny, J. M. Lopez, and A. J. Sieber, "Wide band polarimetric radar inversion studies for vegetation layers," *IEEE Trans. Geosci. Remote Sens.*, vol. 37, no. 5, pp. 2430–2441, Sep. 1999.

[11] S. R. Cloude, "Group theory and polarisation algebra," *Optik*, vol. 75, no. 1, pp. 26–36, 1986.

[12] S. R. Cloude and K. P. Papathanassiou, "Coherence optimization in polarimetric SAR interferometry," in *Proc. IGARSS*, Singapore, 1997, pp. 1932–1934.

[13] W. L. Cameron and L. K. Leung, "Feature motivated polarization scattering matrix decomposition," in *Proc. IEEE Int. Radar Conf.*, Arlington, VA, May 7–10, 1990, pp. 549–557.

[14] E. Krogager, "Aspects of polarimetric radar imaging," Ph.D. dissertation, Tech. Univ. Denmark, Copenhagen, Denmark, May 1993. published Danish Defence Res. Establishment.

[15] E. Krogager and Z. H. Czyz, "Properties of the sphere, diplane, helix decomposition," in *Proc. 3rd Int. Workshop Radar Polarimetry, JIPR*, Nantes, France, Mar. 1995, pp. 106–114.

[16] E. Krogager, "A new decomposition of the radar target scattering matrix," *Electron. Lett.*, vol. 26, no. 18, pp. 1525–1526, Aug. 1990.

[17] J. R. Huynen, "Phenomenological theory of radar targets," Ph.D. dissertation, Tech. Univ. Delft, Delf, The Netherlands, 1970.

[18] R. M. Barnes, "Roll-invariant decompositions of the polarization covariance matrix," Lincoln Lab., M.I.T, Lexington, KY, 1988. Internal Rep.

[19] M. Born and E. Wolf, *Principles of Optics: Electromagnetic Theory of Propagation, Interference and Diffraction of Light*, 7th ed. Cambridge, U.K: Cambridge Univ. Press, 1999.

[20] H. Mott, *Remote Sensing With Polarimetric Radar*. Piscataway, NJ: IEEE Press, 2007.

[21] H. R. Pruppacher and J. D. Klett, *Microphysics of Clouds and Precipitation*. Norwell, MA: Kluwer, 1997.

[22] P. S. Ray, "Broadband complex refractive indices of ice and water," *Appl. Opt.*, vol. 11, no. 8, pp. 1836–1844, 1972.

[23] D. H. O. Bebbington, "Degree of polarization as a radar parameter and its susceptibility to coherent propagation effects," in *Proc. URSI Commission F Symp. Wave Propag. Remote Sens.*, York, U.K., Jun. 1992, pp. 431–436.

[24] D. H. O. Bebbington, R. McGuinness, and A. R. Holt, "Correction of propagation effects in S-band circular polarization-diversity radars," *Proc. Inst. Electr. Eng.*, vol. 134H, no. 5, pp. 431–437, Oct. 1987.

[25] D. H. O. Bebbington, "Target vectors: Spinorial concepts," in *Proc. 2nd Int. Workshop Radar Polarimetry*, Nantes, France, Sep. 1992, pp. 26–36.

[26] G. Brussaard, "Rain-induced crosspolarisation and raindrop canting," *Electron. Lett.*, vol. 10, no. 20, pp. 411–412, Oct. 1974.

[27] M. Chandra, Y. M. Jain, and P. A. Watson, "Assessment of the influence of drop oscillations on dual polarization radar measurements," in *Proc. ICAP*. Norwich, U.K., 1983, pp. 34–39. Preprints, IEE Publ. 219.

[28] A. Hendry, G. C. McCormick, and B. L. Barge, "The degree of common orientation of hydrometeors observed by polarization diversity radars," *J. Appl. Meteorol.*, vol. 15, no. 16, pp. 633–640, Jun. 1976.

[29] A. Hendry, G. C. McCormick, and B. L. Barge, "Ku-band and S-band observations of the differential propagation constant in snow," *IEEE Trans. Antennas Propag.*, vol. AP-24, no. 4, pp. 521–525, Jul. 1976.

[30] C. Lopez-Martinez and X. Fabregas, "Polarimetric SAR speckle noise model," *IEEE Trans. Geosci. Remote Sens.*, vol. 41, no. 10, pp. 2232–2242, Oct. 2003.

[31] E. M. Kennaugh, "Polarization dependence of RCS—A geometrical interpretation," *IEEE Trans. Antennas Propag.*, vol. AP-29, no. 2, pp. 412–413, 1981.

[32] J. R. Saylor and B. K. Jones, "The existence of vortices in the wakes of simulated raindrops," *Phys. Fluids*, vol. 17, no. 3, p. 031 706, Mar. 2005.

[33] M. Galletti, D. H. O. Bebbington, M. Chandra, and T. Boerner, "Fully polarimetric analysis of weather radar signatures," in *Proc. 2008 IEEE Radar Conf.*, Rome, Italy, May 2008, pp. 561–566.

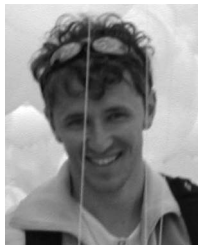

Michele Galletti received the Laurea degree in physics (110/110 e lode) from the Alma Mater Studiorum Università di Bologna, Bologna, Italy, in 2003.

In 2004 and 2005, he was a Scientist with the European Union-funded Project Application of Multiparameter Polarimetry in Environmental Remote Sensing, working on the applications of radar polarimetry. Since 2006, he has been with the Microwaves and Radar Institute, German Aerospace Center, Wessling, Germany.

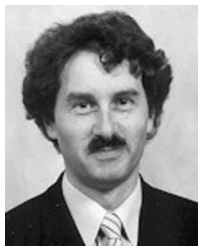

David H. O. Bebbington received the B.A. degree in experimental and theoretical physics and the Ph.D. degree in radio astronomy from Cambridge University, Cambridge, U.K., in 1977 and 1986, respectively.

From 1981 to 1984, he was with the Rutherford Appleton Laboratory, working on millimeter wave propagation research. Since 1984, he has been with the University of Essex, Colchester, U.K., where he currently holds the post of Senior Lecturer in the Department of Electronic Systems Engineering. His interests are polarimetry, applications of wave propagation in remote sensing, and weather radars.

Madhu Chandra received the B.Sc. degree in mathematics from the University of London, London, U.K., in 1978 and the Ph.D. degree in physics from the University of Salford, Salford, U.K., in 1981.

In 1980, he was a Member of the academic staff with the Department of Electrical Engineering, University of Bradford, Bradford, West Yorkshire, U.K. In 1984, he was with the Microwaves and Radar Institute, German Aerospace Center, Wessling, Germany. Since April 2002, he has been a Full Professor and the Head of the Department of Microwave Engineering and Photonics, Chemnitz University of Technology, Chemnitz, Germany. He is the Chairman of the national and international URSI Commission F and the German Information Technology Society (ITG) Committee for wave propagation.

Thomas Börner received the Diploma degree in physics from the University of Munich, Munich, Germany, 1996 and the Ph.D. degree in geography (remote sensing), in 2000.

Since 2005, he has been the Head of the Propagation and Scattering Group, Microwaves and Radar Institute, German Aerospace Center, Wessling, Germany. His current activities are the management and scientific supervision of quality assessment of synthetic aperture radar (SAR) data (SARCON; CALIX), and the studies about atmospheric propagation effects in weather radar and SAR data.